GeoConvention
Calgary • Canada • March 7-11 2016
OPTIMIZING RESOURCES

Moment tensor inversion for the induced earthquakes in the Western Canadian Sedimentary Basin

Hongliang Zhang, David W. Eaton
Department of Geoscience, University of Calgary

Summary

Earthquake source mechanisms can provide important clues to discriminating between natural and induced events. In this study, we calculate moment tensors of one **M** 5.3 natural event and eight induced earthquakes with magnitudes ranging between **M** 3.2 and **M** 4.4 in the Western Canadian Sedimentary Basin to investigate physical differences between natural and induced earthquakes. In addition to a dominant double-couple component, most induced events exhibit significant non-double-couple components within the inverted moment tensor. The presence of multiple fractures and the dilatant jogs created at the overlapping areas of multiple fractures or pre-existing faults may contribute to the larger isotropic and compensated linear vector dipole components respectively.

Introduction

A great number of studies have attempted to characterize the source properties of both the induced and natural earthquakes. In the sense of moment tensor, it is well known that the natural tectonic earthquakes are expected to have nearly pure double-couple (DC) component and small non-DC components [Julian et al., 1998; Miller et al., 1998]. However, in the case of induced earthquakes, this relationship is less clear. Complex source rupture mechanisms have been reported for induced earthquakes in geothermal fields, with mixed non-DC and shear motions that could be related to rapid fluid flow accompanying crack opening near the injection well [Ross et al., 1996; Guilhem et al., 2014]. The presence of significant non-DC component can be taken as a strong indicator for induced events of some certain types (e.g. collapse or rock burst) [Cesca et al., 2013], and the non-negligible isotropic component of the earthquakes associated with fluid injection suggests the simultaneous source volume changes [Zhao et al., 2014].

The motivation for this study is to improve our understanding of the source properties of induced seismicity, and to develop robust criteria to discriminate induced seismicity from natural tectonic earthquakes based on moment tensors. Nine earthquakes in the Western Canadian Sedimentary Basin (WCSB) are investigated, which consist of 8 induced earthquakes detected from July 2014 to June 2015 with magnitudes ≥ **M** 3 and one inferred **M** 5.3 natural earthquake. The moment tensors based on the waveform fitting method are otained and analyzed in this study.

Theory

Under a point-source approximation, the displacement in the *n* direction at location **x** and time *t* can be expressed by [Stump and Johnson, 1977]

$$u_n(\mathbf{x},t) = M_{pj}[G_{np,j} * s(\tau)] \quad , (1)$$

where M_{pj} is the force couple which consists of two opposite forces acting in the ±*p* directions, separated by a distance along *j* direction representing the element of the seismic moment tensor **M**. $G_{np,j}$ represents the spatial derivative of the Green's function G_{np} in *j* direction, and *s*(*t*) is the source time function. The summation convention is used here and the asterisk denotes convolution.

In the frequency domain, equation (1) can be written in linearized form as

$$u_n(\mathbf{x}, f) = M_{pj}(f)G_{np,j}(f) \quad . (2)$$

Based on this expression, the forward problem can be cast in matrix notation as

$$\mathbf{u} = \mathbf{G}\bar{\mathbf{m}} \quad , (3)$$

where **u** is a vector with sampled values of observed ground displacement, **G** is a $n \times 6$ matrix containing the Green's functions computed using an appropriate velocity model and **m** is a vector with 6 elements of the moment tensor. Inversion of equation (3) to obtain the moment tensor elements can be solved by a generalized least-squares method [Jost and Herrmann, 1989].

After inversion, the moment tensor is initially decomposed into two parts: an isotropic term (ISO), which is associated with the volumetirc change, and a remaining deviatoric component. The initial decomposition is unique. Then the deviatoric component can be decomposed in several ways [Jost and Herrmann, 1989]. In this study, we represent the deviatoric part by a double-couple (DC) and compensated linear vector dipole (CLVD) [Knopoff and Randall, 1970; Fitch et al., 1980].

Dataset

The targeted area outlined by red lines in Figure 1 is in the WCSB, which is considered to be a low-seismicity region with no previous major destructive earthquakes [Lamontagne et al., 2008]. However, with the increasingly active energy resource development in this region, the seismicity rate has increased in the past 30 years, and over 250 earthquakes of M $\geqslant$ 3 were detected [Atkinson et al., 2015]. Most of the earthquakes were found to be associated with hydraulic fracturing and wastewater disposal as shown in Figure 1. The nine earthquakes considered here are marked by flags in Figure 1. The origin times, hypocentral locations, and event magnitudes are listed in Table 1. The inferred natural M 5.3 event that occurred east of Dawson Creek, B.C. on 14 April 2001 caused no reported structural damage. The other eight induced earthquakes were detected between July 2014 and June 2015 with magnitudes ranging from M 3.2 to M 4.4, and relatively shallow focal depths. The eight induced events are mainly distributed in the Crooked Lake cluster (events 6, 7, 9), the Rocky Mountain House cluster (events 2, 5, 8) and the Montney cluster (events 3, 4).

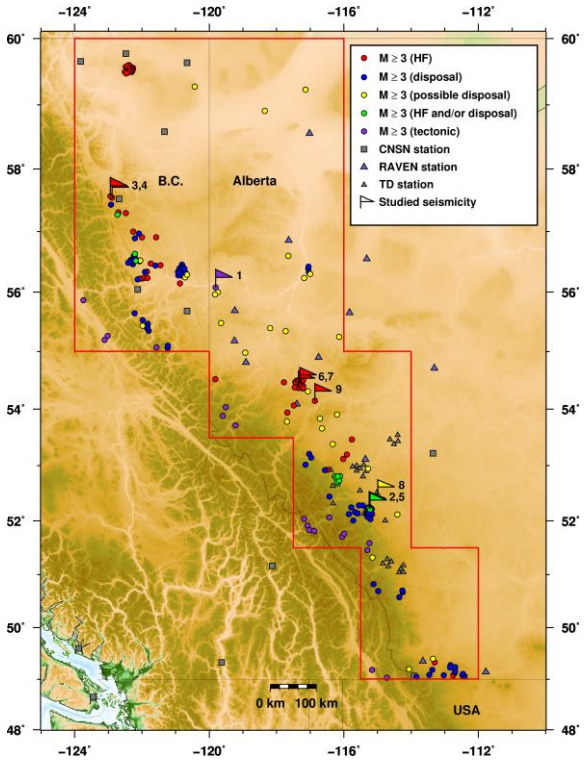

Figure 1. Earthquakes of M ≥ 3 from 1985 to June 2015 and network configuration in the study area (outlined by red lines).

Moment tensor inversion

To minimize the effect of long-period noise (e.g. ground noise) and high-frequency scattered waves, different frequency bands of 0.01-0.025 Hz are selected for the natural event and 0.045-0.075 Hz for induced events. Both the raw data and the Green's functions are filtered by a 3-pole causal bandpass Butterworth filter. The full moment tensor, focal depth and moment magnitude obtained for the nine events are summarized in Table 1. In general, the induced earthquakes exhibit relatively shallow focal depths ranging 2-8 km, which are much shallower than the typical range of the focal depths for the intraplate earthquakes in Canadian Shield. Figures 2 show one example of the complete inversion results (13 June 2015). In general, relative fitness measures for most events exceeded 50 % as shown in Table 1, but we speculate that the vertical and lateral deviation in seismic velocity from the 1D model in some local areas, as well as the relatively large epicentral distances, could reduce the fitness values for some events (e.g. events on 30 July 2014, 4 August 2014).

Figure 3 shows the Hudson's diagram and the percentage of each component after the complete moment tensor decomposition for each of the nine events listed in Table 1. In terms of the natural earthquake in 2001, the focal mechanism is dominated by the DC (81%) accompanied by minor CLVD (14%) and ISO (5%), which suggests that it is well represented as by a pure shear faulting mechanism with a negligible volumetric component, as expected for a shear failure on a 2D fault surface. However, with one exception, the induced events exhibit significant deviatoric components (Figure 3). The only induced event with a comparable DC dominant mechanism (85%) occurred on 4 August 2014.

Table 1. Source parameters resulting from the moment tensor inversion.

Event ID	Date	Time (UTC)	Goodness of fit (%)	Depth (km)	Mw	Moment tensor	Fault planes for best DC (strike, dip, rake)
1	2001/04/14	02:20:13.000	73.7	15	5.2		I. 18, 45, 99 II. 275, 46, 81
2	2014/07/13	09:12:01.560	50.9	6	3.2		I. 111, 23, 45 II. 339, 74, 107
3	2014/07/30	21:23:56.000	24.4	4	3.7		I. 128, 55, -81 II. 293, 36, -102
4	2014/08/04	17:17:24.000	27.6	2	4.0		I. 24, 6, 148 II. 146, 87, 85
5	2014/08/09	15:28:51.000	46.7	4.5	3.6		I. 119, 25, 50 II. 342, 71, 106
6	2015/01/14	16:06:25.000	50.0	5.5	3.5		I. 175, 76, 163 II. 269, 73, 14
7	2015/01/23	06:49:20.010	53.3	4.5	3.7		I. 176, 83, 135 II. 273, 46, 10
8	2015/06/02	14:34:50.550	50.6	4	3.1		I. 87, 64, 65 II. 313, 35, 131
9	2015/06/13	23:57:53.000	62.2	8	4.1		I. 101, 75, 46 II. 356, 46, 159

The non- negligible ISO component, including both fracture opening and closing, can be explained by the presence of fluids injected at depth which can create more conductive fluid pathways compared with pure shear cracks. Previous studies demonstrate that, during stimulation process, the induced events with higher ISO component always occur close to the injection wells due to the complicated stress conditions [Zhao et al., 2014; Aker et al., 2014]. Nguyen et al. [1998] noted that the dilatant jog-type damage could be formed at the overlapping and interacting fault tips. The area of maximum dilation was found to be located in the areas where two or more faults interact, and the lowest differential stresses and principal stresses also occur in the same region [Zhang et al., 2008], thus the volume change (dilation or contraction) at the tips or the jogs of the multiple fractures could possibly cause the significant ISO component with positive and negative values representing fracturing opening and closing. The higher proportion of CLVD mechanism can be caused by the cracks opening and propagating under tension, or can be interpreted by the fracture complexity resulting from the fluid injection. During hydraulic fracturing or wastewater disposal, high fluid pressure can reactivate many pre-existing faults or create new fractures,

and many pure shear cracks in parallel failing at nearly the same time can produce CLVD mechanisms [Julian et al., 1998].

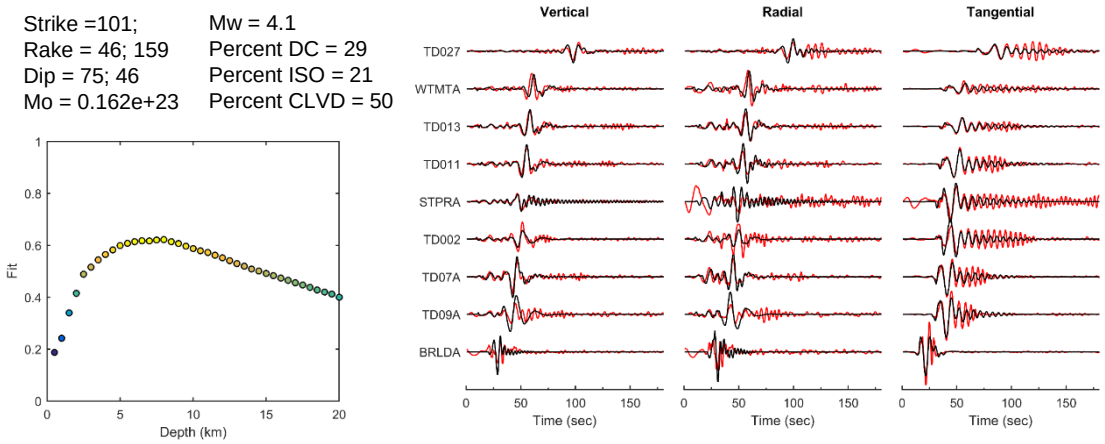

Figure 2. Moment tensor inversion results for the 13 June 2015 event.

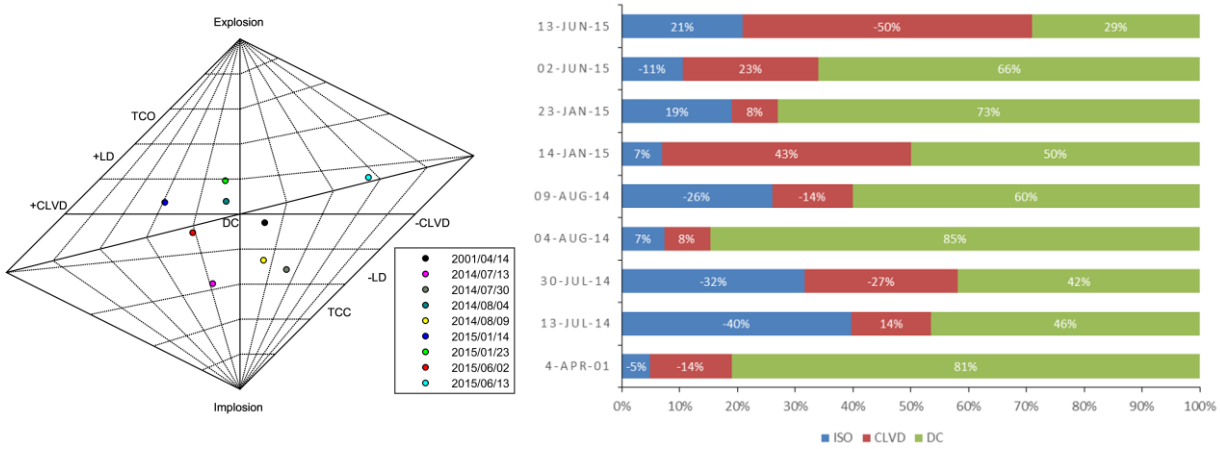

Figure 3. Hudson's diagram and the decomposition of the moment tensor into double-couple (DC, green), compensated linear vector dipole (CLVD, red), and isotropic components (ISO, blue) calculated for each event in **Table 1**.

Conclusions

We calculate the full moment tensors solutions and static stress drop values for nine earthquakes in WCSB including one inferred natural earthquake and eight events triggered by fluid injection during hydraulic fracturing or wastewater disposal. The moment tensor inversion estimates both the focal depth and moment magnitude. Compared with the natural earthquake, the induced events show relatively shallower focal depths ranging from 2 km to 8km which are close to, or slightly deeper than the fluid injection depth. What's more, instead of a DC-dominant (~81%) moment tensor like the natural earthquake, the induced ones show significant non-DC components of up to 71%. We interpret the ISO component of non-DC moment tensors as being caused primarily by dilatantional jogs at zones of overlapping fracture tips opened due to high fluid pressure during injection. We also interpret CLVD components as resulting from the cracks opening and propagating under tension or the combined effects of the multiple parallel shear fractures being either created or re-activated on pre-existing faults.

Acknowledgements

The waveform data used in this study is downloaded from IRIS (http://www.iris.edu/hq/) and NRCan (https://www.nrcan.gc.ca/), and parts of the data from TD network are provided by Nanometrics. This work is supported by TransAlta Utilities, Nanometrics, NSERC, and the Microseismic Industry Consortium.

References

Aker, E., D. Kühn, V. Vavryčukc, M. Soldal, and V. Oye (2014), Experimental investigation of acoustic emissions and their moment tensors in rock during failure, Int. J. Rock. Mech. Min. Sci., 70, 286-295, doi: 10.1016/j.ijrmms.2014.05.003.

Atkinson, G. M., D. W. Eaton, H. Ghofrani, D. Walker, B. Cheadle, R. Schultz, R. Shcherbakov, K. Tiampo, J. Gu, R. M. Harrington, Y. Liu, M. van der Baan and H. Kao (2015), Hydraulic fracturing drives induced seismicity in the Western Canada Sedimentary Basin, submitted, Nature Scientific Reports.

Cesca, S., A. Rohr, and T. Dahm (2013), Discrimination of induced seismicity by full moment tensor inversion and decomposition, J. Seismol., 17, 147-163, doi: 10.1007/s10950-012-9305-8.

Fitch, T. J., D. W. McCowan and M. W. Shields (1980), Estimation of the seismic moment tensor from teleseismic body wave data with applications to intraplate and mantle earthquakes, J. Geophys. Res., 85, 3817-3828, doi: 10.1029/JB085iB07p03817.

Guilhem, A., L. Hutchings, D. S. Dreger, and L. R. Johnson (2014), Moment tensor inversions of M ~ 3 earthquakes in the Geysers geothermal fields, California, J. Geophys. Res., 119, 2121-2137, doi: 10.1002/2013JB010271.

Jost, M. L., and R. B. Herrmann (1989), A student's guide to and review of moment tensor, Seismol. Res. Lett., 60, 37-57, doi: 10.1785/gssrl.60.2.37.

Julian, B. R., A. D. Miller, and G. R. Foulger (1998), Non-double-couple earthquakes I. Theory, Rev. Geophys., 36, 525-549, doi: 10.1029/98RG00716.

Knopoff, L. and M. J. Randall (1970), The compensated linear-vector dipole: a possible mechanism for deep earthquakes, J. Geophys. Res. 75, 4957-4963, doi: 10.1029/JB075i026p04957.

Lamontagne, M., S. Halchuk, J. F. Casidy, and G. C. Rogers (2008), Significant Canadian earthquakes of the period 1600-2006, Seismol. Res. Lett., 79, 211-223, doi: 10.1785/gssrl.79.2.211.

Miller, A. D., G. R. Foulger, and B. R. Julian (1998), Non-double-couple earthquakes II. Observations, Rev. Geophys., 36, 551-568, doi: 10.1029/98RG00717.

Nguyen, P., S. F. Cox, L. B. Harris and C. M. Powell (1998), Fault-value behavior in optimally oriented shear zones: an example at the Revenge gold mine Kambalda, Western Australia, J. Struct. Geol., 20, 1625-1640, doi: 10.1016/S0191-8141(98)00054-6.

Ross, A., G. R. Foulger, and B. R. Julian (1996), Non-double-couple earthquakes mechanisms at the Geysers geothermal area, California, Geophys. Res. Lett., 23, 877-880, doi: 10.1029/96GL00590.

Stump, B. W., and L. R. Johnson (1977), The determination of source properties by the linear inversion of seismograms, Bull. Seismol. Soc. Am., 67, 1489-1502.

Zhang, Y., P. M. Schaubs, C. Zhao, A. Ord, B. E. Hobbs, and A. C. Barnicoat (2008), Fault-related dilation, permeability enhancement, fluid flow and mineral precipitation patterns: numerical models, The Geological Society of London, Special Publications, 299, 239-255, doi: 10.1144/SP299.15.

Zhao, P., D. Kühn, V. Oye, and S. Cesca (2014), Evidence for tensile faulting deduced from full waveform moment tensor inversion during the stimulation of the Basel enhanced geothermal system, Geothermics, 52, 74-83, doi: 10.1016/j.geothermics.2014.01.003.